Tong, Cang; Li, Xiangli; Ge, Xingjie; Wang, Haichao; Duanmu, Lin

A fast numerical approach for the horizontal ground heat exchanger

Published in:
Numerical Heat Transfer Part A: Applications

DOI:
10.1080/10407782.2022.2063644

Published: 01/01/2022

Document Version
Peer-reviewed accepted author manuscript, also known as Final accepted manuscript or Post-print

Please cite the original version:
Tong, C., Li, X., Ge, X., Wang, H., & Duanmu, L. (2022). A fast numerical approach for the horizontal ground heat exchanger. *Numerical Heat Transfer Part A: Applications*, *82*(1-2), 8-30. https://doi.org/10.1080/10407782.2022.2063644

A fast numerical approach for the horizontal ground heat exchanger

Cang Tong[a] Xiangli Li[a*] Xingjie Ge[a] Haichao Wang[a,b] Lin Duanmu[a]

[a] Institute of Building Environment and Facility Engineering, Dalian University of Technology, Dalian University of Technology, Dalian116024, China

[b] Department of Mathematics and Systems Analysis, Aalto University, School of Science, P.O. BOX 11100, Aalto, Finland

The corresponding author: Xiangli Li

* E-mail address: lxl@dlut.edu.cn

Abstract: A fast thermal response numerical (TRN) approach for horizontal ground heat exchanger (HGHE) was developed and verified. The shape equivalence methods was used to process the shapes of pipe cross section and elbows, reducing the meshing difficulty and the grid quantity of HGHE. A series of geometric equivalent quantization values were presented. Meanwhile, a semi-analytical equation was derived to reduce the sensitivity of the TRN model to the time step. In the same case, the calculation speed of the TRN model is 38.98 times that of the Fluent model. Furthermore, long-term operations of HGHE were simulated, revealing that the soil around HGHE has good heat recovery properties.

Nomenclature

Latin symbols

A	Cross-sectional area of the pipe, m^2
Cp	Specific heat capacity, J/(kg.K)
cl_{ad}	Length of the semi-circular elbow *ad, m*
CQ	Cooling capacity of heat pump unit, kW
CP	Power consumption of heat pump in cooling condition, kW
d_i	Inner diameter of the circular pipe, m
d_o	Outside diameter of the circular pipe, m
f	Evaporation coefficient
G	Global solar radiation, W/m^2
h	Convective heat transfer coefficient of fluid in the circular pipe, $W/(m^2.°C)$
h_{sur}	Convective heat transfer coefficient between air and soil surface, $W/(m^2.°C)$
HQ	Heating capacity of heat pump unit, kW
HP	Power consumption of heat pump in heating condition, kW
K	Overall heat transfer coefficient from fluid to close soil ,$W/(m^2.°C)$
l_{ab}	Length of line segment *ab, m*
n	Number of values
P	Perimeter of the pipe section, m
Pr	Prandtl number
PL	Phase lag of ground temperature change, days
PC	Power consumption of heat pump unit, kW
q	Heat flux, W/m^2
Q	Heat exchange amount of elbow, W
Q^+	Heat flowing into the micro-body from upstream, W
Q^-	Heat flowing downstream from the micro-body, W
Q^w	Heat transferred from the surrounding soil to the micro-body, W
Re	Reynolds number
r_a	Relative humidity of the air
r_{ei}	Ratio of the actual inlet temperature to the rated inlet temperature of the evaporator
r_{ci}	Ratio of the actual inlet temperature to the rated inlet temperature of the condenser
R	Overall thermal resistance between fluid and the external soil, °C/W
s_i	Inner side length of the square pipe, m
s_o	Outer side length of the square pipe, m
sl_{ad}	Length of the square elbow *ad,* m
$S_{C,ad}$	Additional constant source
$S_{P,ad}$	Additional source
T	Temperature, °C
u	Fluid velocity, m/s
ΔU	internal energy change, W
$X_{s,i}$	*i*-th predicted value
$X_{e,i}$	*i*-th exact value
Δy	Length of a micro-body in y direction, m
y	Pipe axis direction
z	Depth,m

Greek symbols

τ	Time, s
μ	Dynamic viscosity of the fluid, Pa.s
α	Absorptivity of the earth surface
ε	Earth surface's emissivity
σ	Stephan-Boltzmann constant
θ	Excess-temperature, °C

Superscripts

c	Circular pipe
s	Square pipe
0	Last time step
r	Rated

Subscripts

a	Convective heat transfer
air	Air
avg	Average
amp	Amplitude
ad	Adjoining the pipe
c	Heat conduction
e	Evaporation
f	Fluid
l	Long-wave radiation
P	Node P
s	Soil
sur	Ground surface
sky	Sky
sr	Solar radiation
$wall$	Pipe wall

1. Introduction

Ground-coupled heat pump system (GCHPS) with the horizontal ground heat exchanger (HGHE) is an efficient energy supply system. Due to its low installation cost, the GCHPS has been widely used all over the world. HGHE is an important component of the GCHPS. Whether its design is reasonable or not significantly affects the efficiency of the GCHPS. An accurate thermal response model of HGHE is essential for its optimal design.

There are mainly three geometric types of HGHEs: linear, slinky and spiral GHEs. Although the heat transfer capabilities of the three types of HGHEs are different, their basic heat transfer principles are the same. Scholars have developed a series of analytical and numerical thermal response models for them.

For analytical thermal response models, Ingersoll [1] first proposed an infinite heat source model based on Kelvin's line source theory. Similarly, Carslaw and Jaeger [2] developed the cylinder source model. On the basis of C&J model, Deerman and Kavanaugh [3] generated a frequently-used derivative model. Considering that the length of the ground heat exchanger (GHE) is finite, Diao et al. [4] reported a finite line source model that more accords with the actual situation. These models regarded the line source as a set of countless point sources, and integrated the thermal disturbance effect of the point sources on the soil along the line to obtain the line source effect. They were commonly used to calculate the heat transfer of the vertical ground heat exchanger (VGHE), but the development of many thermal response models for HGHE drew on their modeling ideas. Claesson et al.[5] assumed that the heat exchange between HGHE and the surrounding soil is a steady-state process, and proposed a two-dimensional analytical model based on the finite line source model. Fontaine et al. [6] continued Claesson's assumption and established a three-dimensional analytical model based on the finite line source model. Lamarche [7] developed a new finite line source approach on the basis of the Fontaine model. This method divided the linear GHE into multiple small segments, and the temperature and the heat flux distribution along the GHE were obtained. But it still needed to be based on Claesson's assumption, and the heat transfer history (quantity and characteristics) of the GHE was required to be known in advance. Li et al. [8] proposed a three-dimensional ring source model for the slinky HGHE. This model was generated by integrating the point sources on the ring unit of the slinky HGHE.

Xiong et al. [9] improved the Li model, which considered the influence of the local weather changes and the tube wall thermal resistance on slinky GHE. Similarly, Larwa et al. [10] also put forward a ring source model. The slinky HGHE was simplified to multiple rings with the same heat exchange capacity. The pipe wall temperature and the outlet temperature of each ring were calculated in turn. The studies [1-10] indicate that almost all analytical models evolved from the line source model. These models consider that the heat flux along the GHE is uniform. Individual models take into account the variation of heat flux with the pipe axis, but the generality and accuracy of their characterization method are open to question.

For numerical models, two-dimensional models were first developed, followed by more precise three-dimensional models. Compared to analytical models, numerical models can be closer to the actual situation of the HGHE. Especially the three-dimensional numerical model describing the heat transfer process of the HGHE does not require too much simplification. In terms of two-dimensional numerical models, V.C.Mei [11] established a two-dimensional numerical model for a single straight pipe, which only considered radial and tangential heat transfer. Morrison [12] developed a two-dimensional HGHE model and used the nominal temperature to represent the temperature of each single pipe. The model ignored the heat transfer in the pipe axis direction. The models built by Xing et al.[13], Lee et al.[14], Kayaci et al.[15], Ma[16] and Wang[17] had the similar problems. In terms of three-dimensional models, Florides et al. [18] used FlexPDE software to build two three-dimensional models for the GHEs. The working condition time was 50 h. This research compared the outlet temperature of the HGHE and the VGHE under the same condition. Congedo et al. [19] and Habibi et al. [20] developed the three-dimensional models for the units of the linear, slinky and spiral HGHEs on the CFD platform, and compared their heat exchange performance. The longest working condition time is one year. The results showed that the heat exchange per unit soil length of the spiral HGHE was the largest, while the heat exchange per unit tube length of the linear HGHE was the largest. Chong et al. [21] used Fluent software to build a three-dimensional slinky GHE model, and analyzed the heat transfer per unit tube length of the GHE under different geometric parameters. The working condition time is 60 days. Han et al. [22] and Yoon et al. [23, 24] developed three-dimensional models for different HGHEs based on COMSOL software, and discussed the effects of HGHE geometry form, soil physical properties and pipe length, etc. on the heat performance of the HGHEs. The longest working condition time is 120 h. Go et al. [25] employed COMSOL software to perform a series of numerical analyses on the HGHEs. The operating time of the HGHEs is from June to August. The optimal design sizes of HGHE were presented. To conclude this section, it is difficult for the two-dimensional HGHE models to describe the heat transfer characteristics of HGHE accurately, because these models ignore the heat transfer in the axial direction of the pipe. Most existing three-dimensional models that can accurately calculate heat transfer processes are usually built by the commercial software. But the software only has general heat transfer models without acceleration models for HGHE. Furthermore, the arc structure in HGHE makes it more challenging to discretize the grid, and the number of grid elements is commonly the level of millions. For these reasons, the simulation for the HGHE requires a lot of computing resources and time, and the present researches mainly focus on short-term working conditions of the HGHE. This situation is not conducive to the optimal design of the HGHE.

In view of the problems existing in the previous analytical and numerical models, we proposed a new thermal response numerical (TRN) approach balancing the calculation speed and the accuracy to support the optimal design of HGEHs. This work firstly processed the form of the HGHE based on the shape equivalence methods. The circular cross section of pipe and the semi-circular elbow were equivalent to the square cross section and the square elbow, respectively. Their geometric equivalent quantization values were investigated (see section 2.2). Then a semi-analytical equation calculating the fluid temperature inside the HGHE was derived by the integral method. This equation was coupled with the numerical model of the soil domain through the additional source term method. The FORTRAN code corresponding to the TRN model has been programmed (see section 2.3). In the meantime, an experiment was designed and implemented to validate the TRN model (see section 3). Moreover, the calculation speed of the TRN model and the Fluent model were compared through a case (see section 4). Finally, the long-term operating conditions of GCHPS were discussed (see section 5).

2. Model development

Among the three types of HGEHs, the linear HGEH has the least installation cost and installation difficulty, and it can achieve the equal heat exchange capacity of the other two HGEHs by increasing the pipe installation density. Hence, this work chose the linear HGEH as the research object, as shown in Fig.1 (a). The inlet and outlet pipes are usually wrapped with insulation cotton, and the header pipe accounts for a small proportion of the total length of the HGEH. For these reasons, the geometry of the HGEH was simplified (see Fig.1 (a) to Fig.1 (b)): only the heat transfer of the HGEH body was considered.

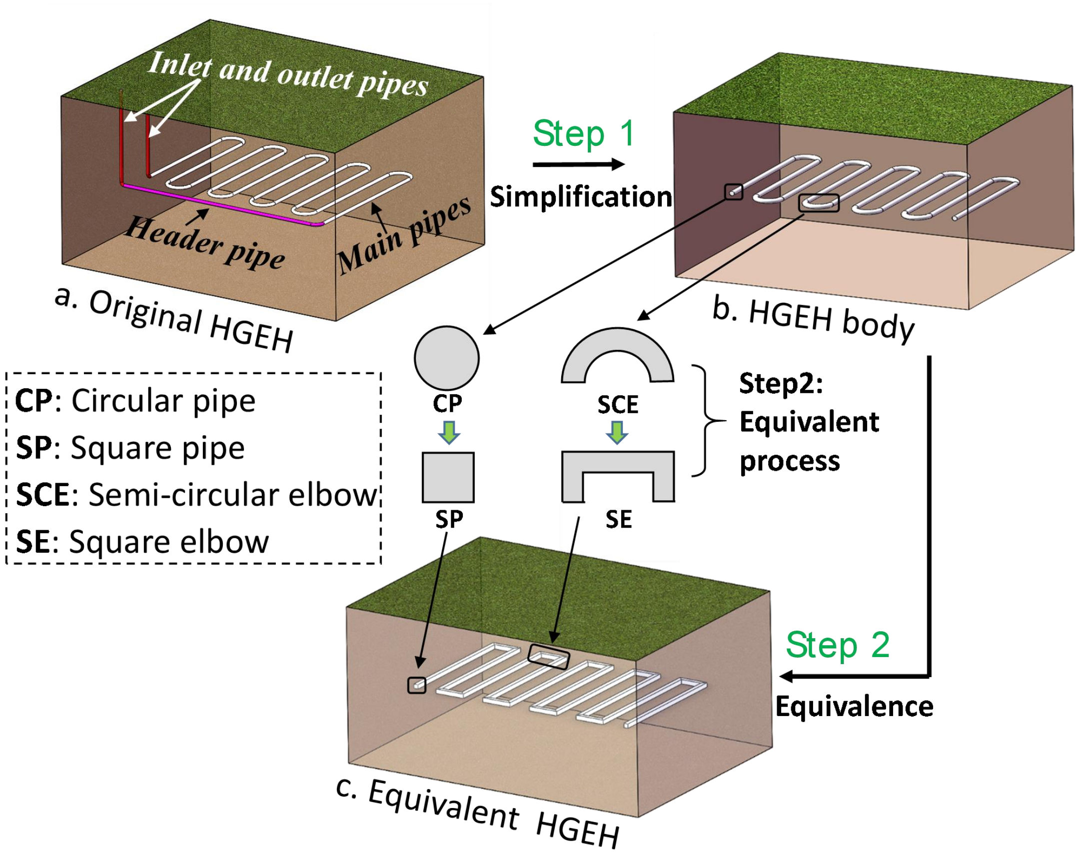

Figure1. Simplified equivalent diagram of HGEH

The HGEH body is mainly composed of straight pipes and elbows. For numerical simulations, meshing the computational domain is essential. In the computational domain, the surrounding soil area is usually a regular cube area, while the pipes have the circular cross-sections and the elbows are arc-shaped. This fact makes it time-consuming and experience-required to divide the mesh of HGEH. To ensure the quality of the grid, the coupling between the pipe and the surrounding soil has to use the refined small unstructured grids to the transition so that the number of grid elements is enormous. As we all know, the number of grid elements is inversely proportional to the calculation speed. In response to this problem, this work used the shape equivalence method to modify the HGEH (see Fig.1 (b) to Fig.1 (c)): On one hand, the circular pipe was equivalent to the square pipe, namely pipe cross-section equivalence; On the other hand, the semi-circular elbow (SCE) was equivalent to the square elbow. After the equivalent treatment, the soil area and the pipe are all cubes, which significantly reduces the meshing difficulty and the grid quantity.

2.1. Heat transfer model for HGHE

The heat transfer mechanism of the circular pipe and the square pipe needs to be clarified for exploring their equivalent geometric relationship. Thus, the heat transfer model of HGHE should be presented. Some assumptions were made before developing the HGEH model as follows:

1. Since the pipe diameter of HGEH is relatively small, the heat transfer inside the fluid is mainly concentrated in the direction of the pipe axis. This work considered the temperature in the cross-section of the fluid is equal and the flow velocity is also the same;

2. The contact thermal resistance between the pipe wall and the adjacent soil is ignored;

3. The physical properties of soil do not change with temperature;

4. The elbow of HGEH is considered as the standard semicircle.

Based on the above assumptions, this work developed the heat transfer models for the HGEH and the surrounding soil. For the HGEH, the internal energy change of the fluid in the pipe is equal to the difference between the incoming and outgoing heat from the outside in a time step. The energy change balance diagram of the two kinds of HGEHs is shown in Fig.2.

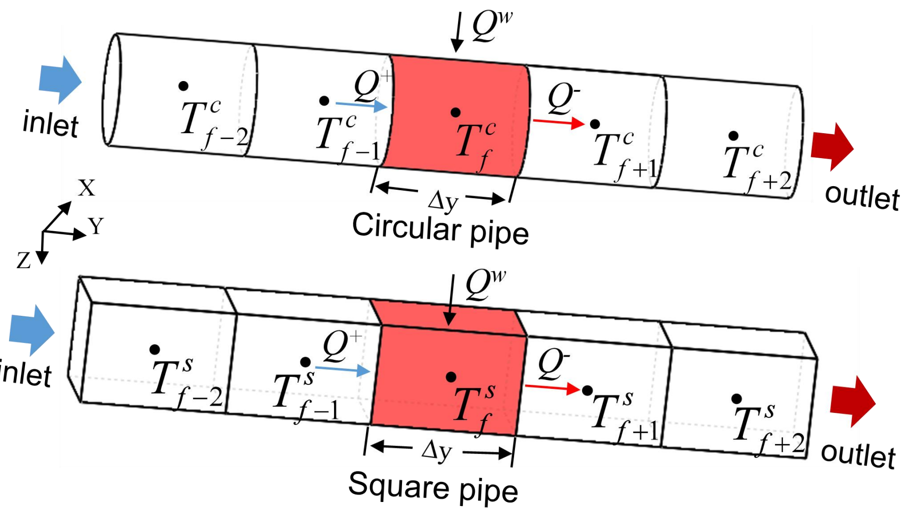

Figure2. Heat transfer process of HGHEs

Take the HGHE with the circular pipe as an example, the energy balance equation is as follows:

$$\Delta U = Q^{+} - Q^{-} + Q^{w} \tag{1}$$

With

$$\begin{cases} \Delta U = \rho_f C_{pf} \dfrac{\partial T_f^c}{\partial \tau} A^c \Delta y \\ Q^{+} = \rho_f C_{pf} A^c u^c T_f^c - \lambda_f A^c \dfrac{\partial T_f^c}{\partial y} \\ Q^{-} = Q^{+} + \dfrac{\partial Q^{+}}{\partial y} \Delta y = Q^{+} + \rho_f C_{pf} A^c u^c \dfrac{\partial T_f^c}{\partial y} \Delta y - \lambda_f A^c \dfrac{\partial^2 T_f^c}{\partial y^2} \Delta y \\ Q^{w} = K^c P^c \Delta y (T_{s,ad}^c - T_f^c) \end{cases} \tag{2}$$

Substituting Eq. (2) into Eq. (1), the energy balance equation can take form, as shown in Eq. (3).

$$\rho_f C_{pf} \frac{\partial T_f^c}{\partial \tau} A^c + \rho_f C_{pf} u^c A^c \frac{\partial T_f^c}{\partial y} = \lambda_f A^c \frac{\partial^2 T_f^c}{\partial y^2} + K^c P^c (T_{s,ad}^c - T_f^c) \tag{3}$$

In a similar way, the energy balance equation for the HGHE with the square pipe, as shown in Eq. (4).

$$\rho_f C_{pf} \frac{\partial T_f^s}{\partial \tau} A^s + \rho_f C_{pf} u^s A^s \frac{\partial T_f^s}{\partial y} = \lambda_f A^s \frac{\partial^2 T_f^s}{\partial y^2} + K^s P^s (T_{s,ad}^s - T_f^s) \tag{4}$$

Where ΔU is the internal energy change of the micro-body (W), Q^{+} is the heat flowing into the micro-body from upstream (W), Q^{-} is the heat flowing downstream from the micro-body (W), Q^{w} is the heat transferred from the surrounding soil to the micro-body (W), ρ_f is the fluid density (kg/m^3), C_{pf} is the fluid specific heat capacity (J/(kg.K)), T_f is the fluid temperature (°C), τ is time(s), A is the cross-sectional area of the pipe (m^2), u is the fluid velocity (m/s), λ_f is the heat conductivity coefficient of the fluid (W/(m.°C)), K is the overall heat transfer coefficient from the fluid to the close soil (W/(m^2.°C)), P is the perimeter of the pipe section (m), $T_{s,ad}$ is the temperature of the soil adjoining the pipe (°C), Δy is the length of a micro-body in y-direction(m), y denotes the pipe axis direction; Superscript c denotes the circular pipe, and superscript s denotes the square pipe.

The heat transfer model in the soil area is as follows.

$$\rho_s C_{ps} \frac{\partial T_s}{\partial \tau} = \frac{\partial}{\partial x}(\lambda_s \frac{\partial T_s}{\partial x}) + \frac{\partial}{\partial y}(\lambda_s \frac{\partial T_s}{\partial y}) + \frac{\partial}{\partial z}(\lambda_s \frac{\partial T_s}{\partial z}) \tag{5}$$

Where ρ_s is the soil density (kg/m^3), C_{ps} is the soil specific heat capacity (J/(kg.K)), λ_s is the heat conductivity coefficient of the fluid (W/(m.°C)), T_s is the soil temperature (°C).

The boundary conditions and the initial condition of the computational domain will be discussed in Section 2.4

2.2. Equivalence process

2.2.1. Equivalence to pipe cross section

This work followed the guideline of the shape equivalence method: before and after the HGHE is equivalent, their heat transfer process should be the same, the fluid temperature in the two pipes as well. For this purpose, each item in Eq. (3) and Eq. (4) should be equal. In other words, the coefficients of the T items in the two equations should be equal. According to this relationship, the relevant parameters of the square pipe can be derived as follows:

1. The internal energy change of the micro-body in a time step should be equal, namely that the coefficients of the unsteady state term in Eq. (3) and Eq. (4) should be the same:

$$\rho_f C_{pf} A^c = \rho_f C_{pf} A^s \tag{6}$$

With

$$\begin{cases} A^c = \dfrac{d_i^{\ 2}}{4}\pi \\ A^s = s_i^{\ 2} \end{cases} \tag{7}$$

Where d_i is the inner diameter of the circular pipe (m), s_i is the inner side of the square pipe (m).

Substituting Eq. (7) into Eq. (6), s_i can be deduced, as shown in Eq. (8).

$$s_i = \frac{\sqrt{\pi}}{2} d_i \tag{8}$$

2. The heat change of the micro-body caused by the fluid flow in a time step should be equal, namely that the coefficient of the convection terms in Eq. (3) and Eq. (4) should be the same:

$$\rho_f C_{pf} u^c A^c = \rho_f C_{pf} u^s A^s \tag{9}$$

u^s can be deduced according to Eq. (9), as shown in Eq. (10).

$$u^s = u^c \tag{10}$$

3. The heat change of the micro-body obtained by thermal diffusion in a time step should be equal, namely that the coefficients of the thermal diffusion terms in Eq. (3) and Eq. (4) are equal:

$$\lambda_f A^c = \lambda_f A^s \tag{11}$$

As with the conclusion obtained in Eq. (6), the cross-sectional area of the two pipes should be equal.

$$A^c = A^s \tag{12}$$

4. The heat change of the micro-body caused by the soil outside the pipe in a time step should be equal, namely that the coefficients of the source terms in Eq. (3) and Eq. (4) are equal:

$$K^c P^c = K^c P^c \tag{13}$$

Eq. (13) can be transformed into Eq. (14), as follows:

$$R^c = \frac{1}{K^c P^c \Delta y} = \frac{1}{K^s P^s \Delta y} = R^s \tag{14}$$

Where R^c and R^s are the overall thermal resistance between the fluids in the circular pipe and in the square pipe and the adjacent soil (°C/W), respectively.

Take the overall thermal resistance R_x between T_f and $T_{i-1,k}$ as an example for illustration, their thermal resistance network is shown in Fig.3. The heat from the soil to the fluid needs to overcome the soil thermal conductivity resistance R_{soil}, the pipe-wall thermal resistance R_{wall} and convective heat transfer resistance R_{water}. Hence, R_x is the sum of the above three thermal resistances, as shown in Eq. (15).

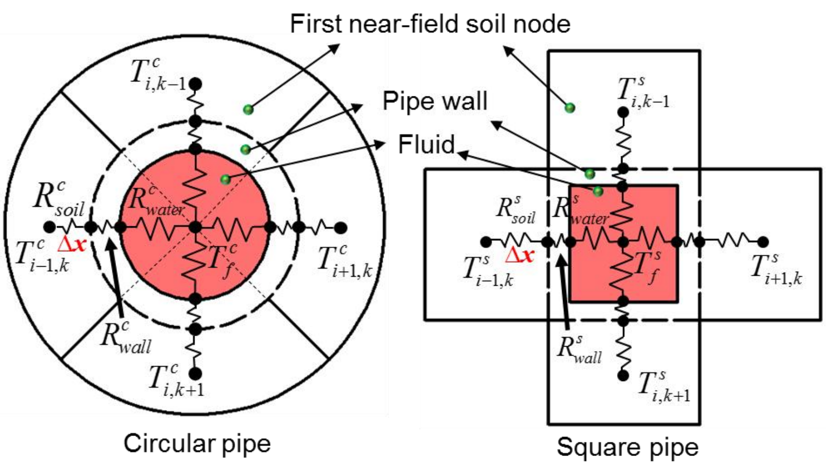

Figure 3. Thermal resistance network between fluid and first near-field soil node

$$\begin{cases} R_x^c = R_{soil}^c + R_{wall}^c + R_{water}^c = \dfrac{\ln((d_o+0.5\Delta x)/d_o)}{\dfrac{2\pi\Delta y}{4}\lambda_s} + \dfrac{\ln(d_o/d_i)}{\dfrac{2\pi\Delta y}{4}\lambda_{wall}} + \dfrac{1}{\dfrac{\pi d_i\Delta y}{4}h^c} \\ R_x^s = R_{soil}^s + R_{wall}^s + R_{water}^s = \dfrac{0.5\Delta x}{\dfrac{(s_o+s_i)}{2}\Delta y\lambda_s} + \dfrac{0.5(s_o-s_i)}{\dfrac{(s_o+s_i)}{2}\Delta y\lambda_{wall}} + \dfrac{1}{s_i\Delta y h^s} \end{cases} \tag{15}$$

Where d_o is the outside diameter of the circular pipe (m), s_o is the outer side length of the square pipe (m), λ_{wall} is the thermal conductivity of the pipe wall (W/(m.°C)). h^c is the convective heat transfer coefficient of fluid in the circular pipe (W/(m^2.°C)), h^s is the convective heat transfer coefficient of fluid in the square pipe (W/(m^2.°C)).

h^c can be calculated by the non-dimensional correlation (Eq. (16))[26].

$$h^c = \begin{cases} \dfrac{3.66\lambda_f}{d_i} & (\mathrm{Re} \le 2300) \\ \dfrac{0.023\lambda_f \mathrm{Re}^{0.8}\mathrm{Pr}^n}{d_i} & (\mathrm{Re} > 2300) \end{cases} \tag{16}$$

With

$$\begin{cases} \mathrm{Re} = \dfrac{u^c\rho_f d_i}{\mu} \\ \mathrm{Pr} = \dfrac{\mu C_{pf}}{\lambda_f} \\ n = 0.3\ (\text{for cooling}) \\ n = 0.4\ (\text{for heating}) \end{cases} \tag{17}$$

Where Re and Pr are Reynolds number and Prandtl number, respectively. μ is the dynamic viscosity of the fluid (Pa.s).

According to Eq. (14)-Eq. (17), the effective convective heat transfer coefficient h^s of the square pipe can be derived, as shown in Eq. (18)

$$h^s = \frac{1}{\dfrac{4s_i}{d_i\pi h} + \dfrac{2s_i\ln(d_o/d_i)}{\pi\lambda_{wall}} - \dfrac{s_i(s_o-s_i)}{(s_o+s_i)\lambda_{wall}} + \dfrac{2s_i\ln((d_o+0.5\Delta x)/d_i)}{\pi\lambda_s} - \dfrac{s_i\Delta x}{(s_o+s_i)\lambda_s}} \tag{18}$$

Additionally, the heat capacity per unit length of the two pipes should be the same, as shown in Eq. (19).

$$\rho_{wall}C_{pwall}\frac{\pi}{4}(d_o^{\,2}-d_i^2) = \rho_{wall}C_{pwall}(s_o^{\,2}-s_i^2) \tag{19}$$

Where ρ_{wall} is the density of pipe wall (kg/m^3), C_{pwall} is the specific heat capacity of pipe wall (J/(kg.K))

s_o can be deduced according to Eq. (19), as shown in Eq. (20).

$$s_o = \sqrt{(\frac{\sqrt{\pi}}{2})^2 ({d_o}^2 - {d_i}^2) + {s_i}^2} \tag{20}$$

So far, the critical parameters of the square pipe, including the effective inner side length s_i, the effective flow velocity u^s, the effective convective heat transfer coefficient h^s and the effective outer side length s_o, are available from Eq. (8), Eq. (10), Eq. (18) and Eq. (20), respectively.

2.2.2. Equivalence to pipe elbow

The HGHE contains many semi-circular elbows adjoined soil, resulting in the difficulty of meshing the computational domain. Compared to the VGHE, the ratio of the elbow length to the total length of HGHE is larger. Ignoring roughly the heat transfer at the elbow will inevitably have an adverse effect on the accuracy of the heat transfer model of HGHE. Thus, this work used the square elbow instead of the semi-circular elbow, and restored the original heat exchange effect of the HGHE as much as possible. The schematic diagram of the equivalent method for the elbows is shown in Fig.4. The length of l_{bc} is equal to the pipe spacing 'D', and it can be not change. Because the pipe spacing is a sensitive factor that affects the heat transfer of HGHE [23], changing the pipe spacing optionally will definitely affect the equivalent effect. However, the length of l_{ab} and l_{bc} is unknown and equal.

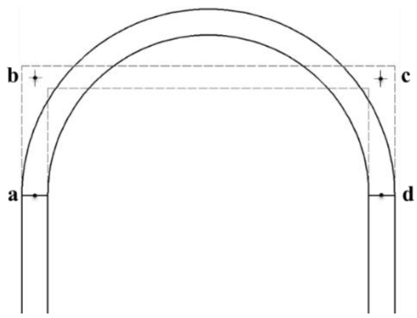

Figure 4. Equivalent schematic diagram of elbows

In order to acquire the lengths of the l_{ab} corresponding to the semi-circular elbows of different lengths, the mirror method was employed here, as shown in Fig.5. Take an elbow unit as the research object, it means that the influence of the semi-circular elbow and the square elbow on the surrounding soil should be the same if the heat exchange amounts of two elbows are equal. In other words, the temperature changes caused by the two elbow heat sources at any position of the surrounding soil are equal.

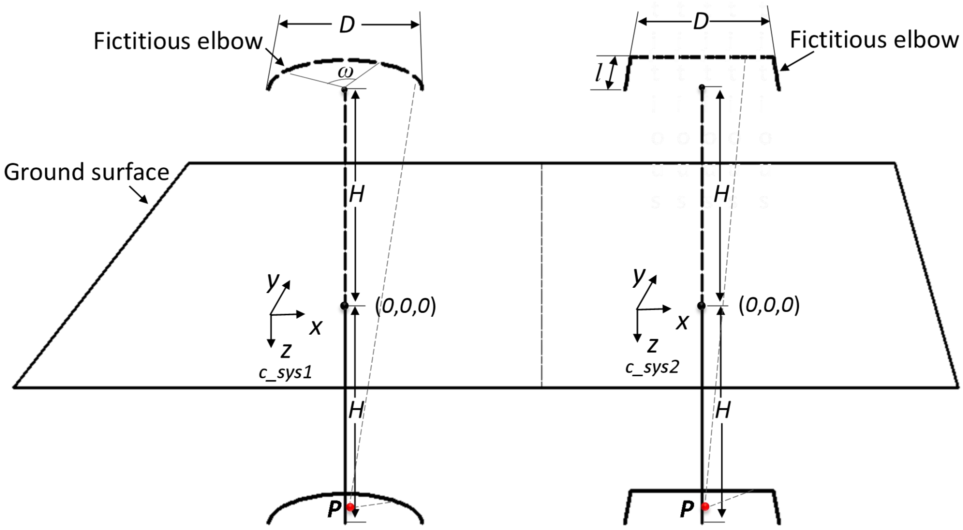

Figure 5. Mirror method for elbows

The soil temperature change caused by the semi-circular elbow heat source was calculated by Eq. (21).

$$\theta^c(\tau)=\frac{Q_{el}}{4\pi^2\lambda_s}\left(\int_0^{\pi}\frac{1}{L(P_{arc},P)}ercf\left(\frac{L(P_{arc},P)}{2\sqrt{a_s\tau}}\right)d\omega-\int_0^{\pi}\frac{1}{L(P'_{arc},P)}ercf\left(\frac{L(P'_{arc},P)}{2\sqrt{a_s\tau}}\right)d\omega\right) \tag{21}$$

With

$$\begin{cases} L(P_{arc},P)=\sqrt{(x-\frac{D}{2}\cos(\omega))^2+(y-\frac{D}{2}\sin(\omega))^2+(z-H)^2} \\ L(P'_{arc},P)=\sqrt{(x-\frac{D}{2}\cos(\omega))^2+(y-\frac{D}{2}\sin(\omega))^2+(z+H)^2} \end{cases} \tag{22}$$

Where θ is the excess-temperature (°C), Q_{el} is the heat exchange amount of the elbow unit (W), L is the distance between any position in the soil and the elbow (m), H is the burial depth of HGHE (m).

Let $\Theta=\frac{4\pi\lambda_s\theta}{Q_{el}}$, $Fo=\frac{a\tau}{D^2}$. Eq. (21) can be transformed into Eq. (23), as follows:

$$\Theta^c(Fo)=\frac{1}{\pi}\left(\int_0^{\pi}\frac{1}{L(P_{arc},P)}ercf\left(\frac{L(P_{arc},P)/D}{2\sqrt{Fo}}\right)d\omega-\int_0^{\pi}\frac{1}{L(P'_{arc},P)}ercf\left(\frac{L(P'_{arc},P)/D}{2\sqrt{Fo}}\right)d\omega\right) \tag{23}$$

Similarly, the influence of the square elbow on the surrounding soil is described by Eq. (24).

$$\Theta^s(Fo) = \frac{1}{(D+2l_{ab})}\left(\int_0^{l_{ab}} \frac{1}{L(P_{lab},P)} ercf\left(\frac{L(P_{lab},P)/D}{2\sqrt{Fo}}\right)ds + \int_{-D/2}^{D/2} \frac{1}{L(P_{lbc},P)} ercf\left(\frac{L(P_{lbc},P)/D}{2\sqrt{Fo}}\right)ds \right.$$
$$+ \int_0^{l_{ab}} \frac{1}{L(P_{lcd},P)} ercf\left(\frac{L(P_{lcd},P)/D}{2\sqrt{Fo}}\right)ds - \int_0^{l_{ab}} \frac{1}{L(P'_{lab},P)} ercf\left(\frac{L(P'_{lab},P)/D}{2\sqrt{Fo}}\right)ds$$
$$\left. - \int_{-D/2}^{D/2} \frac{1}{L(P'_{lbc},P)} ercf\left(\frac{L(P'_{lbc},P)/D}{2\sqrt{Fo}}\right)ds - \int_0^{l_{ab}} \frac{1}{L(P'_{lcd},P)} ercf\left(\frac{L(P'_{lcd},P)/D}{2\sqrt{Fo}}\right)ds\right) \tag{24}$$

With

$$\begin{cases} L(P_{lab},P) = \sqrt{(x+\frac{D}{2})^2 + (y-l)^2 + (z-H)^2} \\ L(P_{lbc},P) = \sqrt{(x-l)^2 + (y-l_{ab})^2 + (z-H)^2} \\ L(P_{lcd},P) = \sqrt{(x-\frac{D}{2})^2 + (y-l)^2 + (z-H)^2} \\ L(P'_{lab},P) = \sqrt{(x+\frac{D}{2})^2 + (y-l)^2 + (z+H)^2} \\ L(P'_{lbc},P) = \sqrt{(x-l)^2 + (y-l_{ab})^2 + (z+H)^2} \\ L(P'_{lcd},P) = \sqrt{(x-\frac{D}{2})^2 + (y-l)^2 + (z+H)^2} \end{cases} \tag{25}$$

Take the centroid of the semi-circle as the typical position, it makes the values of Θ^c and Θ^s at this position equal, namely Eq. (23) = Eq. (24). Then the length of l_{ab} corresponding to the different semi-circular elbow (pipe spacing) can be calculated. The results were presented in Fig.6.

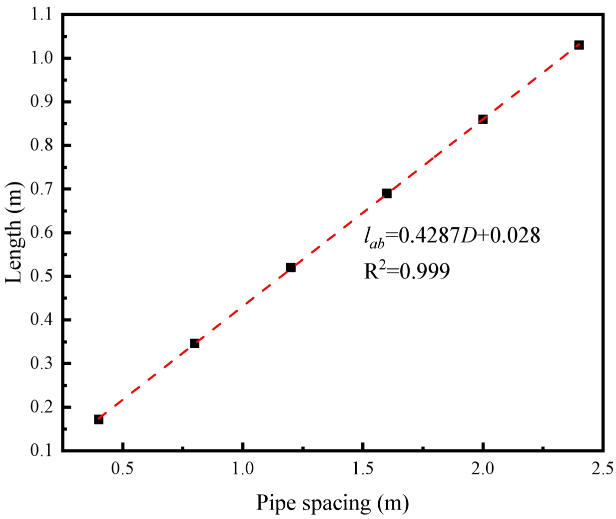

Figure 6. Length of line segment ‘ab’ in different pipe spacing

2.3. A semi-analytical heat transfer model for fluid in the pipe

In the previous section, the calculation speed was prospectively improved by reducing the number of grid elements. The time step size is also an important factor affecting the calculation speed. The heat transfer in the computational domain includes the heat transfer inside HGHE, the heat transfer between the HGHE and the surrounding soil, and the heat transfer of the soil itself. In these heat transfer processes, the heat transfer inside HGHE, which is described by the model (see Eq. (4)), is most susceptible to the influence of time step. Because this model contains a convection term. Thus, this section intends to develop a semi-analytical heat transfer equation for solving the fluid node temperature in the pipe. Its purpose is to reduce the sensitivity of the calculation accuracy to the time step and increase the calculation speed.

Here, the energy balance equation of the square pipe (see Eq. (4)) is integrated into a control volume 'Δy' based on the finite volume method. The result is shown in Eq. (26). For the convenience of writing, the superscript s in the equations is omitted.

$$\rho_f C_{pf} \frac{\partial T_f}{\partial \tau} A\Delta y = \rho_f C_{pf} uA(T_{f-1} - T_f) + \lambda_f A(\frac{T_{f+1} - T_f}{(\partial y)_n} - \frac{T_f - T_{f-1}}{(\partial y)_s}) + KP\Delta y(T_s - T_f) \tag{26}$$

Where $(\partial y)_s$ is the distance between the micro-body node and the node of the adjoining upstream micro-body. $(\partial y)_n$ is the distance between the micro-body node and the node of the adjoining downstream micro-body.

Then the unsteady term in Eq. (27) is integrated into a time step Δt:

$$\int_{T_P^0}^{T_P} \frac{\rho_f C_{pf} A\Delta y}{\rho_f C_{pf} uA(T_{f-1} - T_f) + \lambda_f A(\frac{T_{f+1} - T_f}{(\partial y)_n} - \frac{T_f - T_{f-1}}{(\partial y)_s}) + KP\Delta y(T_s - T_f)} dT_f = \int_t^{t+\Delta t} d\tau \tag{27}$$

Where T_P is the temperature of the micro-body in this time step (°C), and T_P^0 is the temperature of the micro-body in the last time step (°C).

The solution to Eq. (27) is:

$$T_P = \frac{(1 - e^{-\frac{\beta}{\gamma}\Delta t})\alpha + \beta e^{-\frac{\beta}{\gamma}\Delta t} T_P^0}{\beta} \tag{28}$$

With

$$\begin{cases} \alpha = \rho_f C_{pf} uAT_{f-1} + \lambda_f A(\frac{T_{f+1}}{(\delta y)_n} + \frac{T_{f-1}}{(\delta y)_s}) + KP\Delta y T_s \\ \beta = \rho_f C_{pf} uA + \lambda_f A(\frac{1}{(\delta y)_n} + \frac{1}{(\delta y)_s}) + KP\Delta y \\ \gamma = \rho_f C_{pf} A\Delta y \end{cases} \tag{29}$$

The temperature of the nodes in the fluid can be solved by Eq. (28). The coupling boundary between the pipe and the soil is processed by the additional source term method. Take the node P in the pipe for illustration, the discrete general equation of the fluid area is expressed in Eq. (30)

$$a_P T_P = a_N T_N + a_S T_S + b \tag{30}$$

With

$$a_N = (1 - e^{-\frac{\beta}{\gamma}\Delta t}) \frac{\lambda_f \Delta x \Delta z}{(\delta y)_n} \tag{31}$$

$$a_S = (1 - e^{-\frac{\beta}{\gamma}\Delta t})(\rho_f \Delta x \Delta z C_{p,f} u + \frac{\lambda_f \Delta x \Delta z}{(\delta y)_s}) \tag{32}$$

$$a_P = \rho_f C_{p,f} u \Delta x \Delta z + \lambda_f C_{p,f} (\frac{1}{(\delta y)_s} + \frac{1}{(\delta y)_n}) - S_{P,ad} \Delta V \tag{33}$$

$$a_P^0 = \beta e^{-\frac{\beta}{\gamma}\Delta t} \tag{34}$$

$$b = a_P^0 T_P^0 + S_{C,ad} \Delta V \tag{35}$$

$$\Delta V = \Delta x \Delta y \Delta z \tag{36}$$

$$\begin{aligned} S_{C,ad} = \frac{1}{\Delta V}\Bigg(& \frac{(1 - e^{-\frac{\beta}{\gamma}\Delta t}) T_W}{(\frac{1}{h' s_i \Delta y} + \frac{s_w - s_i}{\lambda_{wall}(s_w + s_i)\Delta y} + \frac{\Delta x_W}{\lambda_s (s_w + s_i)\Delta y})} + \frac{(1 - e^{-\frac{\beta}{\gamma}\Delta t}) T_E}{(\frac{1}{h' s_i \Delta y} + \frac{s_w - s_i}{\lambda_{wall}(s_w + s_i)\Delta y} + \frac{\Delta x_E}{\lambda_s (s_w + s_i)\Delta y})} \\ & + \frac{(1 - e^{-\frac{\beta}{\gamma}\Delta t}) T_U}{(\frac{1}{h' s_i \Delta y} + \frac{s_w - s_i}{\lambda_{wall}(s_w + s_i)\Delta y} + \frac{\Delta z_U}{\lambda_s (s_w + s_i)\Delta y})} + \frac{(1 - e^{-\frac{\beta}{\gamma}\Delta t}) T_D}{(\frac{1}{h' s_i \Delta y} + \frac{s_w - s_i}{\lambda_{wall}(s_w + s_i)\Delta y} + \frac{\Delta z_D}{\lambda_s (s_w + s_i)\Delta y})}\Bigg) \end{aligned} \tag{37}$$

$$\begin{aligned} S_{P,ad} = -\frac{1}{\Delta V}\Bigg(& \frac{1}{(\frac{1}{h' s_i \Delta y} + \frac{s_w - s_i}{\lambda_{wall}(s_w + s_i)\Delta y} + \frac{\Delta x_W}{\lambda_s (s_w + s_i)\Delta y})} + \frac{1}{(\frac{1}{h' s_i \Delta y} + \frac{s_w - s_i}{\lambda_{wall}(s_w + s_i)\Delta y} + \frac{\Delta x_E}{\lambda_s (s_w + s_i)\Delta y})} \\ & + \frac{1}{(\frac{1}{h' s_i \Delta y} + \frac{s_w - s_i}{\lambda_{wall}(s_w + s_i)\Delta y} + \frac{\Delta z_U}{\lambda_s (s_w + s_i)\Delta y})} + \frac{1}{(\frac{1}{h' s_i \Delta y} + \frac{s_w - s_i}{\lambda_{wall}(s_w + s_i)\Delta y} + \frac{\Delta z_D}{\lambda_s (s_w + s_i)\Delta y})}\Bigg) \end{aligned} \tag{38}$$

Where T_P, T_W, T_E are the temperatures of the fluid nodes (°C), T_N, T_S, T_U, T_D are the temperatures of the soil nodes outside the wall (°C), $S_{C,ad}$ and $S_{P,ad}$ are the additional source terms.

Based on the above methods and models, this work developed a program for simulating the heat transfer of HGHE based on FORTRAN code and Visual Basic. The program employs an implicit solver and uses the alternate direction Gauss–Seidel iteration method to solve the nodal equation set. More importantly, this program realizes the automatic division of the computational domain grid. Just requiring a few parameters like the size of the HGHE and the growth rate of the grid size, the division of the global grid and the heat transfer calculation are expected to be completed. The operation interface of the program for meshing and a grid example are shown in Fig.7. It dispenses with the traditional process: geometric modeling, then meshing and finally solving. This dramatically reduces the time cost to divide the grid and solve.

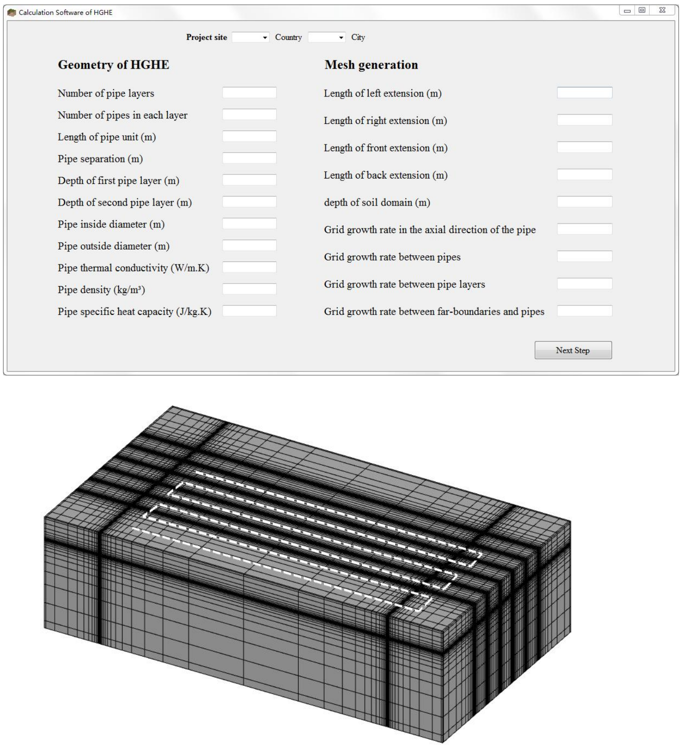

Figure 7. Part of the procedure interface and a mesh example

2.4. Boundary condition and initial condition

HGHE is installed in shallow ground. The soil temperature field is significantly affected by the surface weather conditions, such as solar radiation (SR), heat convection (HC), surface evaporation (SE) and long-wave radiation (LR). At present, many studies [7, 20, 27, 28] introduced Kusada correlation and used it as the top boundary condition and the initial condition of the HGHE model. However, Kusada correlation [29] was developed by pure heat conduction theory and ignored radiation heat transfer, convective heat transfer and evaporation heat transfer. It is hard for Kusada correlation to characterize the interaction between the external meteorological factors and soil. Kusada correlation used in the HGHE model leads to the inevitable error. Therefore, this work intends to replace Kusada correlation with higher-precision boundary conditions and initial condition.

In our previous study [30], we developed and experimentally verified a heat balance equation (see Eq. (39)) which comprehensively considered the influence of four factors, including solar radiation, long-wave radiation between the sky and the surface, convective heat transfer between air and the surface, and surface evaporative heat transfer, on the ground temperature. Then a series of two-harmonic analytical correlations (THACs) was proposed for predicting the ground temperature profiles in many cities (see Eq. (41)). Simultaneously, a comparison indicated that the accuracy of THAC is much higher than that of Kusada correlation. Thus, this work used the heat balance equation as the top boundary and adopted the THAC as the initial condition of the calculation domain. Its four sides are adiabatic boundaries, and the bottom is a constant temperature boundary, as illustrated in Fig. 8.

$$q_c = -\lambda_s \left.\frac{\partial T_s}{\partial z}\right|_{z=0} = q_s - q_l + q_a - q_e \tag{39}$$

With

$$\begin{cases} q_s = \alpha G \\ q_l = \varepsilon\sigma((T_{sur}+273.15)^4 - {T_{sky}}^4) \\ q_a = h_{sur}(T_{air} - T_{sur}) \\ q_e = cfh_{sur}[(aT_{sur}+b) - r_a(aT_{air}+b)] \end{cases} \tag{40}$$

Where q_c is the heat conduction from the surface to the interior (W/m^2), q_s is the solar radiation absorbed by the surface (W/m^2), q_l is the long-wave radiation between the sky and the surface (W/m^2), q_a is convective heat transfer between the air and the surface (W/m^2), q_e is the evaporation heat exchange of ground surface (W/m^2). z denotes the depth (m), T_{sur}, T_{sky}, T_{air} are the ground surface temperature (°C), the sky temperature (°C) and the air temperature (°C), respectively. α is the absorptivity of the earth surface, G is the global solar radiation (W/m^2), ε is the earth surface's emissivity and σ is the Stephan-Boltzmann constant (5.67*10^{-8} W/m^2·K^4), h_{sur} is the convective heat transfer coefficient between air and soil surface (W/(m^2.K)), a, b and c are 103 (Pa/K), 609 (Pa) and 0.0168 (K/Pa), respectively. r_a is the relative humidity of the air, f is the evaporation coefficient.

$$T_s(z,\tau) = \begin{Bmatrix} T_{s,avg} - T_{amp1} * e^{-z\sqrt{\frac{\pi}{a_s t_p}}} \cos\left[\frac{2\pi}{t_p}(\tau - PL_1) - z\sqrt{\frac{\pi}{a_s t_p}}\right] \\ -T_{amp2} e^{-z\sqrt{\frac{2\pi}{a_s t_p}}} \cos\left[\frac{2\pi * 2}{t_p}(\tau - PL_2) - z\sqrt{\frac{2\pi}{a_s t_p}}\right] \end{Bmatrix} \tag{41}$$

Where $T_{s,avg}$ is the average soil temperature of the area (°C), T_{amp1} and T_{amp2} are the ground temperature amplitudes (°C), PL_1 and PL_2 are the phase lag of ground temperature change (days).

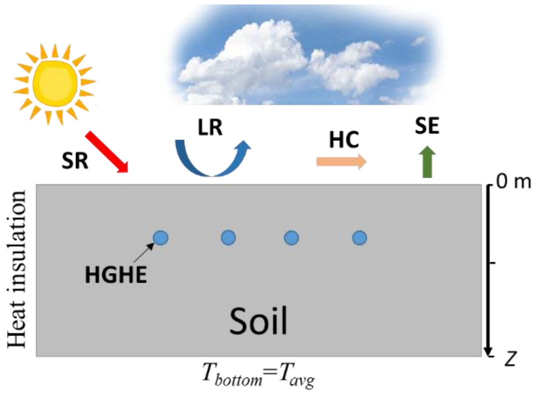

Figure 8. Boundary conditions for the computational domain

3. Model validation

The HGHE experiment was implemented to assess the accuracy of the TRN model. The experimental facility includes a HGHE laid in a yellow sand-filled container, a water bath, a flow meter, a NI temperature measuring device and several Pt1000 thermal resistance sensors, as shown in Fig.9. The HGHE length is 9.3 m and the installation depth is 0.5 m. The material of the HGHE is Polyethylene (PE), and the outer diameter of the pipe is 25 mm, and the thickness of the pipe wall is 2.0 mm. The medium in the pipe is water. The main thermal properties of the experimental facility are shown in Table 2. Moreover, the length, width and height of the container are 2.1 m, 2.2 m and 1.5m, respectively. Its four side walls were wrapped with the insulation cotton for heat insulation. The water bath was regarded as a load simulator. The NI temperature measuring device and several Pt1000 thermal resistance sensors were used to test the temperature in the experimental facility. The precision of the Pt1000 thermal resistance sensor is 0.01°C.

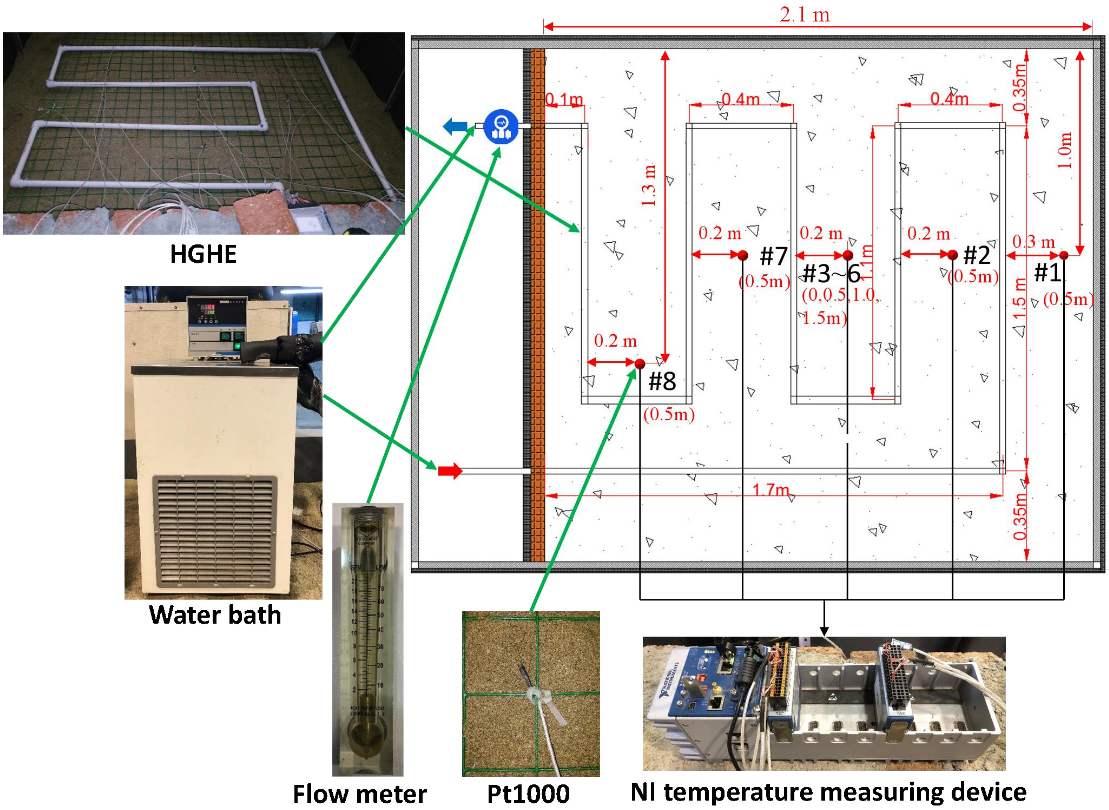

Figure 9. Schematic diagram of the experimental platform

Table2. Thermal properties of the experimental facility

Items	Thermal conductivity (W/(m.K))	Density (kg/m^3)	Specific heat capacity (J/kg.K)	Viscosity (Pa.s)
Sand	0.9	1500	1600	-
PE	0.35	946	1920	-
Water	0.6	998.2	4182	0.001003

In the test condition, the heating and cooling conditions were successively carried out one after another by adjusting the water temperature of the water bath. The water flow velocity was 0.12 m/s. The top temperature of the sand measured by the PT1000 sensors was 20.8°C, and the initial temperature was 20.01°C. The observed inlet temperature of the HGHE was assigned to the TRN model, and then the outlet temperature of the HGHE was calculated. The outlet temperature and the temperature of P2 from the TRN model and the experiment were compared, as illustrated in Fig.10. The root mean squared error (RMSE) was introduced to evaluate the accuracy. The RMSE expression is shown in Eq. (42). RMSEs of the outlet temperature and the temperature of P2 are 0.5°C and 0.1°C, respectively. Whether it is heating or cooling conditions, the hourly simulated value is well agreement with the hourly observed value. This indicates that the TRN model has good accuracy.

$$RMSE = \sqrt{\frac{\sum_{i=1}^{n}(X_{s,i} - X_{e,i})^2}{n}} \tag{42}$$

Where $X_{s,i}$ and $X_{e,i}$ are the i-th predicted value and the i-th exact value, respectively; n is the number of values.

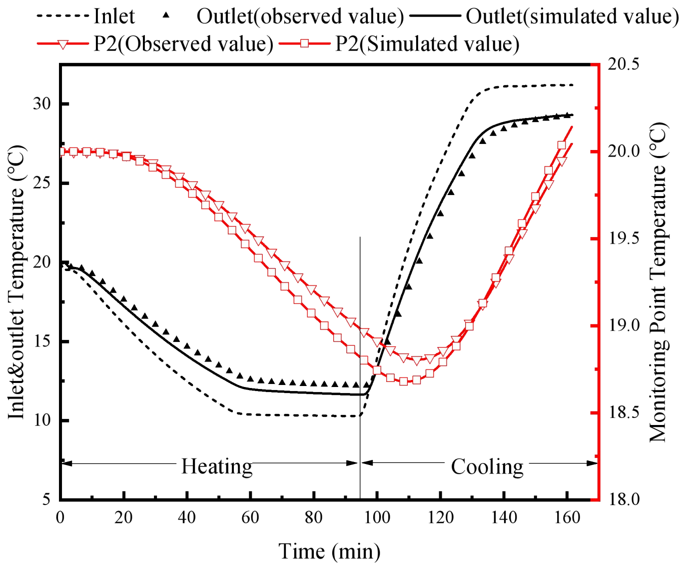

Figure10. Observed and simulated temperature of the HGHE

4. Comparison of the TRN model and the Fluent model

In order to prove the calculation efficiency of the TRN model, this work compared it with the model developed by Fluent software based on the same case. The case was designed as follows: the HGHE with a length of about 136 m is located in Dalian, China. Both its pipe spacing and buried depth are 2 m. The pipe material of HGHE is PE. The outer diameter of the pipe and the thickness of the pipe wall are 32 mm and 2.3 mm, respectively. The fluid in the pipe is water, and the flow velocity is 0.3 m/s. The HGHE undertakes a constant load of 2036W. The thermal conductivity, density and specific heat capacity of the soil are 1.9 W/(m.K), 1700 kg/m^3 and 2253 J/(kg.K), respectively.

For the Fluent model, its definite conditions were set by the user-defined functions (UDF). Then the grid and the time-step independence of the Fluent model were verified to ensure its accuracy. Four scenarios with different mesh numbers were set (see Fig.11 a). The mesh number was reduced from 7.03 million to 2.48 million. When the grid quantity is not less than 3.46 million, the average outlet temperatures of the HGHE in the corresponding scenarios are relatively close. However, when the mesh number is reduced to 2.48 million, the average outlet temperature of the HGHE has a significant drift compared with the previous three scenarios. Similarly, six scenarios with different time steps were set (see Fig.11 b). When the time step is not greater than 60 s, the average outlet temperatures and the temperature change trends of the HGHE in these scenarios were approximate, but when the time step increases further, the average outlet temperatures of the HGHE have a significant deviation compared with the previous scenarios. In other words, 'Δτ=60 s' is a turning point. Therefore, the grid quantity and the time step of the Fluent model were determined to be 3.62 million and 60 s, respectively. The grid diagram of the Fluent model is shown in Fig.12.

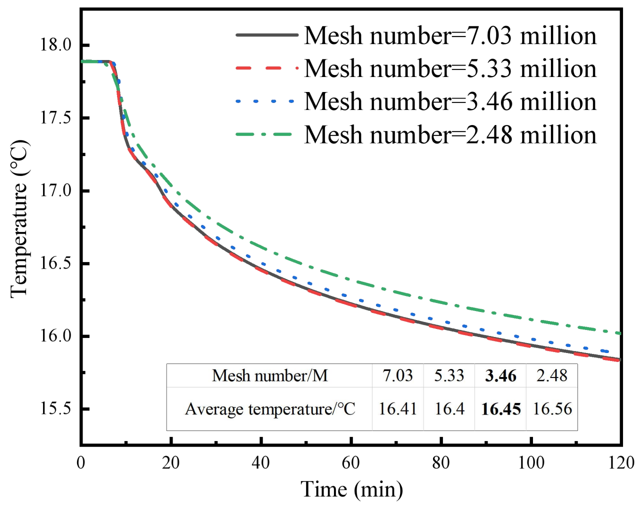

a. Mesh independence

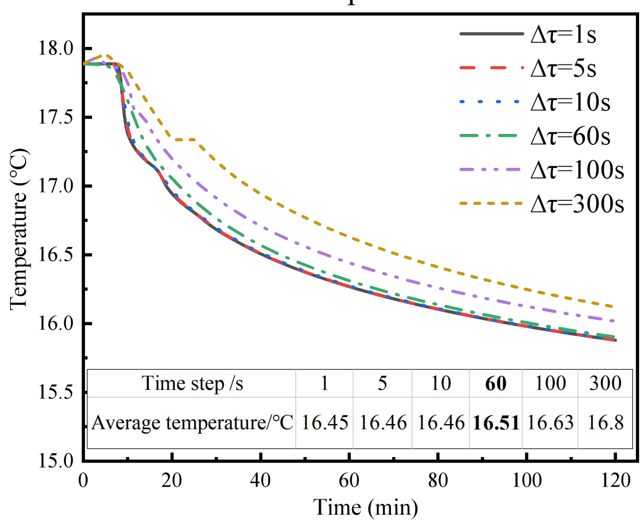

b. Time step independence

Figure 11. Hourly outlet temperature in different scenarios

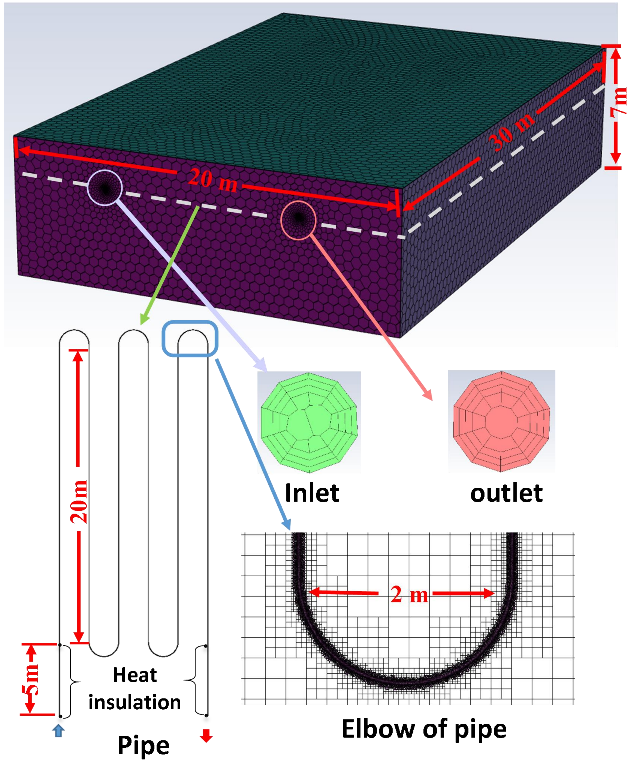

Figure 12. Mesh of the Fluent model

The above-mentioned case was calculated based on the TRN model and the Fluent model, respectively. A single-core solver was used for calculations. The configuration of the computer employed is that CPU is Intel Core i5-4460 CPU@3.20GHz, and the random-access memory is 32 GB. Six different time steps ranging from 10 s to 1200 s were first set, and then these conditions of the TRN model were calculated sequentially. The outlet temperature of the HGHE was monitored. In terms of mesh quantity, the TRN model only required 548 thousand grids, which is about 15.1% of the mesh number of the Fluent model. For computational accuracy, Fig.13 shows the outlet temperature change trends during 48 hours of operation. It is seen that the results calculated by the two models are basically consistent. Take the results calculated by the Fluent model as the benchmark solution, the RMSEs of the outlet temperature calculated by the TRN model in different time steps were summarized in Table 3. Table 3 demonstrates that the errors of the work conditions corresponding to the time step of 10 s, 60 s and 300 s are very close. When the time step is 600 s or 900 s, the errors increase slightly. However, when the time step is 1200 s, the error grows significantly. As to the CPU time, the Fluent model requires 19.1 h of CPU time, while the TRN model requires at most 10.1 h and at least 0.4 h, which is inversely proportional to the time step. The calculation speeds of the TRN model have been improved to different degrees compared with that of the Fluent model. This is because the grid quantity required by the TRN model has dropped significantly, and the stability of the calculation to the time step has been improved. Considering the calculation accuracy and CPU time comprehensively, this study deems that the time step of 900s is the best compromise, which is 15 times larger than the time step of the Fluent model. Under this scenario, the calculation speed of the TRN model is increased by 38.98 times that of the Fluent model, which achieved a good acceleration calculation effect.

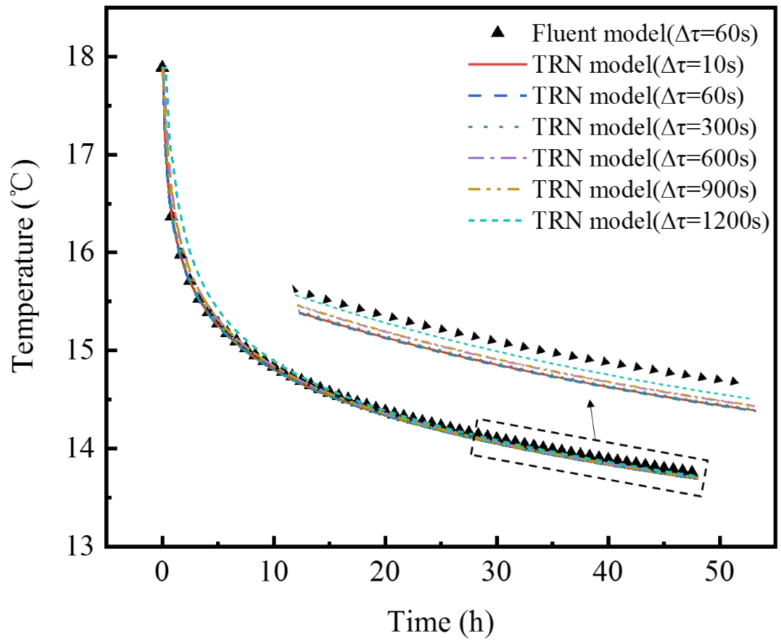

Figure 13. Hourly outlet temperature of the TRN model and the Fluent model

Table 3. Results calculated by TRN model compared with the Fluent model

Items	Time step（s）					
	10	60	300	600	**900**	1200
RMSE(°C)	0.036	0.038	0.039	0.048	**0.054**	0.131
CPU time（h）	10.1	4.6	1.3	0.7	**0.49**	0.4
Increase rate of calculation speed	1.89	4.15	14.69	27.29	**38.98**	47.75

5. Evaluation of long-term operations of GCHPS with HGHE

This section briefly discussed the performance of the heat pump system and the soil heat recovery during long-term operation to provide a reference for similar projects.

A GCHPS with HGHE was designed to provide heating/cooling service for a rural building in Dalian city (cold region). As is well-known, the floor space of HGHE is the biggest obstacle restricting the use of GCHPS. Therefore, the floor space is an important constraint condition for the design of GCHPS. For Chinese rural buildings, the plot ratio generally does not exceed 0.5. In other words, the rural buildings usually have a yard with an acreage not less than the building area. HGHE can be installed in the underground area of the yard. Both the areas of the above-mentioned building and its yard are about 265m^2. The building load is shown in Fig. 14. It can be seen that the heating-cooling load ratio of the building is 2.83:1.

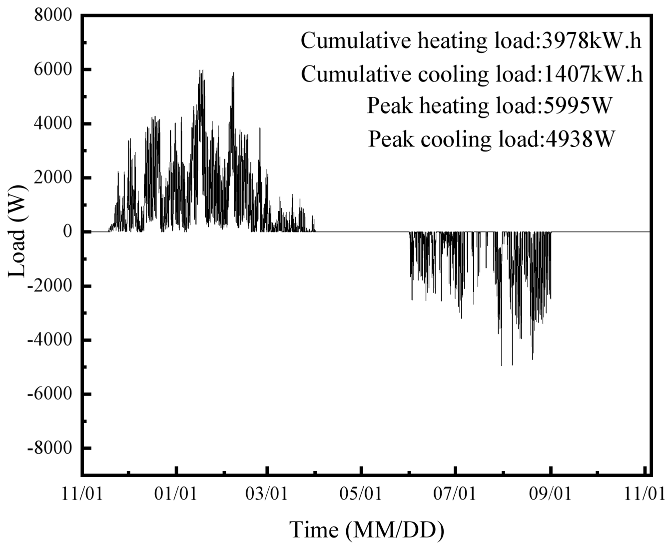

Figure 14. Hourly load of the building

According to the basic information of the building, a HGHE with a length of about 310m was designed and installed 3 m underground. The HGHE includes 20 straight pipes and 19 elbows. The length of each straight pipe is 14 m, and the pipe spacing is 1 m. In consequence, the HGHE covers an area of 266 m^2, which basically satisfies the constraint of the floor space. In addition, the GCHPS employed a high-efficiency heat pump unit (HPU), and its performance correction formulas were fitted, as shown in Eq. 43. The detailed information of the GCHPS matched with the HGHE was summarized in Table 4.

$$\begin{cases} HQ = HQ^r(1.726r_{ei} + 0.540r_{ei}^2 + 2.841r_{ci} + 0.209r_{ci}^2 - 2.707r_{ei}r_{ci} - 1.648) \\ CQ = CQ^r(6.044r_{ei} - 1.749r_{ei}^2 + 0.267r_{ci} + 0.174r_{ci}^2 - 0.897r_{ei}r_{ci} - 2.861) \\ HP = HP^r(0.399r_{ei} + 0.612r_{ei}^2 + 1.518r_{ci} + 0.877r_{ci}^2 - 1.696r_{ei}r_{ci} - 0.713) \\ CP = CP^r(5.795r_{ei} - 1.324r_{ei}^2 + 0.627r_{ci} + 0.411r_{ci}^2 - 1.419r_{ei}r_{ci} - 3.153) \end{cases} \tag{43}$$

Where HQ, CQ, HQ^r, and CQ^r are the actual heating capacity and the actual cooling capacity, the rated heating capacity and the rated cooling capacity of HPU (kW), respectively. HP, HP^r, CP and CP^r are the actual power consumption and the rated power consumption of HPU in heating condition and in cooling condition (kW), respectively. r_{ei} denotes the ratio of the actual inlet temperature to the rated inlet temperature of the evaporator, r_{ci} denotes the ratio of the actual inlet temperature to the rated inlet temperature of the condenser.

Table4. Details of GCHPS

Items	Value
Rated heating capacity of HPU (kW)	6
Rated cooling capacity of HPU (kW)	5
Rated COP for heating mode	4.08
Rated COP for cooling mode	6.00
Rated heating temperature (°C)	45
Rated cooling temperature (°C)	7
Flow of HGHE for heating mode (m/s)	0.5
Flow of HGHE for cooling mode (m/s)	0.4
Length of HGHE (m)	310
Spacing of HGHE (m)	1
Burial depth of HGHE (m)	3
External diameter of HGHE (mm)	32
Wall thickness of HGHE (mm)	2.3
Length of a straight pipe in HGHE(m)	14
Number of the straight pipes	20
Number of HGHE elbows	19

Based on the TRN model, the 10-years operating conditions of the GCHPS were simulated. The inlet and outlet temperatures of the HGHE are shown in Fig.15. It can be seen that whether it was heating or cooling conditions, the inlet and outlet temperature of the HGHE decreased to varying degrees. For the heating season, the minimum inlet temperature of the HGHE was reduced from 4.17°C to 4.08°C, with a decrease of 0.09°C. Similarly, the maximum inlet temperature in the cooling season was reduced from 24.22°C to 24.16°C, with a decline of 0.06°C. This is because the large heating-cooling load ratio causes the accumulation of cold in the soil after the long-term operation of HGHE. However, during the transition seasons, the inlet and outlet temperature of HGHE indirectly reflecting the temperature of the surrounding soil gradually restored to the original soil temperature. From the fourth year, the inlet and outlet temperature of HGHE is not decreasing. This reveals that the heat given by the top boundary to the soil and the heat extracted by HGHE from the soil have regained the heat balance performance. In other words, the shallow soil has good heat recovery. Furthermore, the COP of the HPU for the first heating season is 3.76, and the following 9 years are all 3.75; the COP of the cooling season during the last 10 years is 6.16. This concludes that the ratio of the heat extracted from the soil by the

HGHE to the heat injected into the soil by the HGHE is 1.79:1. In this situation, GCHPS can still maintain stable performance during its lifetime.

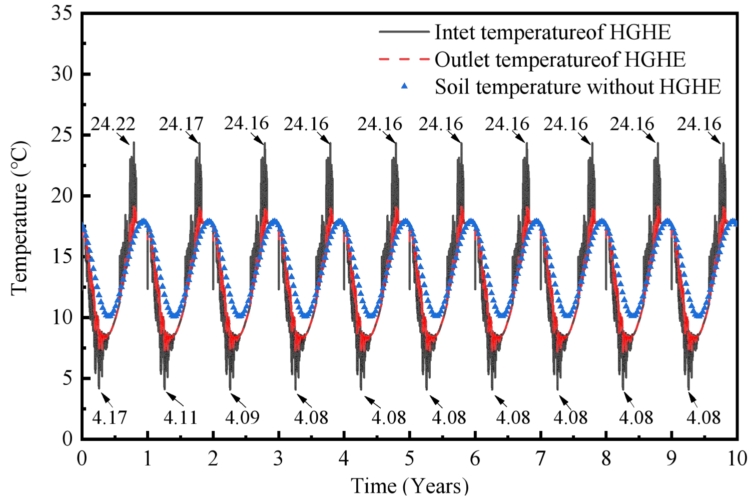

Figure 15. Inlet and outlet temperatures of the HGHE under heating and cooling conditions

In order to further study the heat recovery performance of the soil around the HGHE, this work simulated another working condition where the GCHPS only supplied heat to the building. The cooling load of the building is eliminated by increasing the ventilation. The result of GCHPS running for 10 years is shown in Fig.16. It demonstrates that the minimum inlet temperature of the HGHE was reduced from 4.17°C to 3.86°C, with a drop of 0.31°C. The inlet and outlet temperature of HGHE decreased slightly in the first four years, and the temperature remained basically stable in the following years, and the soil reached a new heat balance. Furthermore, the COPs of the HPU for the first and second heating seasons are 3.76 and 3.75, respectively. The following 8 years are all 3.74. In addition, compared with VGHE [31], the soil around HGHE has better heat recovery performance. When designing HGHE, there is no need to pay too much attention to the cold accumulation problem.

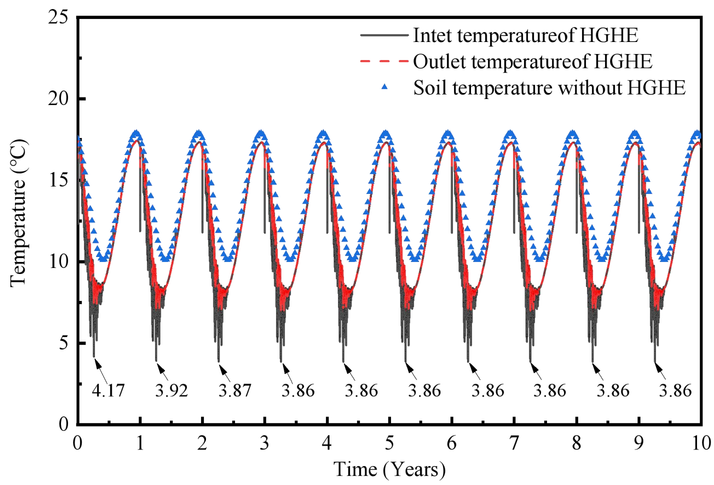

Figure 16. Inlet and outlet temperatures of the HGHE under heating conditions

6. Conclusions

A thermal response numerical model for HGHE was developed in this paper. The meshing difficulty and the grid quantity required by the TRN model were significantly reduced with the help of the shape equivalence method. In the TRN model, the temperature of the fluid in HGHE was calculated by the derived semi-analytical equation, and then the coupling boundary between the fluid and the soil was processed by the additional source term method. Simultaneously, more accurate definite conditions were used in the TRN model. The experiment was carried out to validate the TRN model. Based on a case study, the mesh number required by the TRN model and the Fluent model were compared as well as their calculation speed. Moreover, the long-term operations of GCHPS with HGHE were simulated to reveal the performance of the GCHPS and heat recovery of the surrounding soil. The main conclusions are as follows:

(1) For the same case, the mesh quantity required in the TRN model is only 15.1% of that in the Fluent model. The grid of the TRN model can be automatically divided by the HGHE program with only a few necessary parameters.

(2) According to the derived semi-analytical equation, the TRN model reduces the influence of the time step on the accuracy and implements the simulation under large time steps. When the time step does not exceed 900s, the model can guarantee the accuracy of the calculation.

(3) After improving the mesh number and the time step, the calculation speed of the TRN model is 38.98 times faster than that of the fluent model under the same

condition.

(4) In the case of a heating-cooling load ratio of 2.8:1, the minimum inlet temperature of HGHE has only decreased by 0.09°C in the first four years, and remains stable in the subsequent years. The heating COP of the HPU drops from 3.76 to 3.75, while the cooling COP of the HPU is always 6.16. Even when the HPU only performs heating, the minimum inlet temperature of HGHE only drops by 0.31°C, and the COP dropped from 3.76 to 3.74. That is to say, it is not necessary to pay too much attention to the cold accumulation of soil when designing HGHE.

The novel contribution of this study is to provide a fast and accurate calculation model for simulating the long-term conditions of HGHE and supporting its optimal design. The future work is the parallelization of the TRN model to further increase the computation speed.

Acknowledgements

This study was supported by the National Natural Science Foundation of China (Grant No. 52078097).

References:

[1]. Ingersoll, L.R.P.H., Theory of ground pipe heat source for the heat pump. Heating Piping and Air Conditioning, 1948(20): p. 119-122.

[2]. Carslaw, H.S. and J.C. Jaeger, Conduction of Heat in Solids (2nd ed.). 1959, Oxford: Clarendon Press.

[3]. Deerman, J.D. and S.P. Kavanaugh, Simulation of vertical U-tube ground-coupled heat pump systems using the cylindrical heat source solution. Ashrae Transactions, 1991. 97(1): p. 287-295.

[4]. Diao, N.R., H.Y. Zeng and Z.H. Fang, Improvement in Modeling of Heat Transfer in Vertical Ground Heat Exchangers. HVAC&R Research, 2004. 10(4): p. 459-470.

[5]. Claesson, J. and A. Dunand, Heat extraction from the ground by horizontal pipes — a mathematical analysis. 1983: Byggforskningsrådet (BFR). 215.

[6]. Fontaine, P., et al., Modeling of horizontal geoexchange systems for building heating and permafrost stabilization. Geothermics, 2011(40): p. 211 – 20.

[7]. Lamarche, L., Horizontal ground heat exchangers modelling. Applied Thermal Engineering, 2019. 155: p. 534-545.

[8]. Li, H., K. Nagano and Y. Lai, A new model and solutions for a spiral heat exchanger and its experimental validation. International Journal of Heat and Mass Transfer, 2012. 55(15-16): p.

4404-4414.
[9]. Xiong, Z., D.E. Fisher and J.D. Spitler, Development and validation of a Slinky(TM) ground heat exchanger model. Applied Energy, 2015. 141: p. 57-69.
[10]. Larwa, B. and K. Kupiec, Determination of pipe wall temperature in a slinky-coil ground heat exchanger. International Journal of Heat and Mass Transfer, 2020. 160: p. 120202.
[11]. Mei, V.C., Theoretical heat pump ground coil analysis with variable ground farfield boundary conditions. AIChE Journal, 1986. 32(7): p. 1211-1215.
[12]. Morrison, A., Finite difference model of a spiral ground heat exchanger for ground-source heat pumps. 1998, University of Waterloo.
[13]. Xing, L., et al., Foundation heat exchangers for residential ground source heat pump systems-Numerical modeling and experimental validation. HVAC&R Research, 2011. 17(6): p. 1059-1074.
[14]. Lee, E.S., D.E. Fisher and J.D. Spitler, Efficient Horizontal Ground Heat Exchanger Simulation with Zone Heat Balance Integration. HVAC&R Research, 2013. 19(3): p. 307-323.
[15]. Kayaci, N. and H. Demir, Numerical modelling of transient soil temperature distribution for horizontal ground heat exchanger of ground source heat pump. Geothermics, 2018. 73: p. 33-47.
[16]. Ma, Z., et al., Numerical simulation on heat transfer inside and outside of vertical buried pipes based on two-model order reduction methods. Numerical Heat Transfer, Part A: Applications, 2021. 79(9): p. 631-655.
[17]. Wang, C., et al., A simplified semi-numerical model to simulate a U-pipe ground heat exchanger. Numerical Heat Transfer, Part A: Applications, 2020. 77(5): p. 482-496.
[18]. Florides, G., et al., Modeling and assessment of the efficiency of horizontal and vertical ground heat exchangers. Energy, 2013. 58: p. 655-663.
[19]. Congedo, P.M., G. Colangelo and G. Starace, CFD simulations of horizontal ground heat exchangers: A comparison among different configurations. Applied Thermal Engineering, 2012. 33-34: p. 24-32.
[20]. Habibi, M. and A. Hakkaki-Fard, Evaluation and improvement of the thermal performance of different types of horizontal ground heat exchangers based on techno-economic analysis. Energy Conversion and Management, 2018. 171: p. 1177-1192.
[21]. Chong, C.S.A., et al., Simulation of thermal performance of horizontal slinky-loop heat exchangers for ground source heat pumps. Applied Energy, 2013. 104: p. 603-610.
[22]. Han, C., et al., Influence of local geological data on the performance of horizontal ground-coupled heat pump system integrated with building thermal loads. Renewable Energy, 2017. 113: p. 1046-1055.
[23]. Yoon, S., et al., Significance evaluation of performance factors on horizontal spiral-coil ground heat exchangers. Journal of Building Engineering, 2021. 35: p. 102044.
[24]. Kim, M., et al., Thermal performance evaluation and parametric study of a horizontal ground heat

exchanger. Geothermics, 2016. 60: p. 134-143.
[25]. Go, G., et al., Optimum design of horizontal ground-coupled heat pump systems using spiral-coil-loop heat exchangers. Applied Energy, 2016. 162: p. 330-345.
[26]. Incropera, F., et al., Fundamentals of Heat and Mass Transfer. 2007.
[27]. Pu, L., et al., Structure optimization for horizontal ground heat exchanger. Applied Thermal Engineering, 2018. 136: p. 131-140.
[28]. Habibi, M. and A. Hakkaki-Fard, Long-term energy and exergy analysis of heat pumps with different types of ground and air heat exchangers. International Journal of Refrigeration, 2019. 100: p. 414-433.
[29]. Kusuda, T. and P. Achenbach, Earth Temperature and Thermal Diffusivity at Selected Stations in the United States. ASHRAE Trans., 1965. 71: p. 233.
[30]. Tong, C., et al., Prediction of the temperature profiles for shallow ground in cold region and cold winter hot summer region of China. Energy and Buildings, 2021. 242: p. 110946.
[31]. You, T., et al., An overview of the problems and solutions of soil thermal imbalance of ground-coupled heat pumps in cold regions. Applied Energy, 2016. 177: p. 515-536.